Vaccine 30 (2012) 4095–4105

Contents lists available at SciVerse ScienceDirect

Vaccine

journal homepage: www.elsevier.com/locate/vaccine

Natural killer cell mediated pathogenesis determines outcome of central nervous system infection with Venezuelan equine encephalitis virus in C3H/HeN mice

Katherine Taylor[a], Olga Kolokoltsova[a], Michael Patterson[a], Allison Poussard[a], Jennifer Smith[a], D. Mark Estes[b], Slobodan Paessler[a,*]

[a] Sealy Center for Vaccine Development, Galveston National Lab, Department of Pathology, University of Texas Medical Branch, Galveston, TX 77550, USA
[b] Department of Infectious Diseases, University of Georgia College of Veterinary Medicine, Athens, GA 30602, USA

ARTICLE INFO

Article history:
Received 21 December 2011
Received in revised form 7 March 2012
Accepted 25 March 2012
Available online 21 April 2012

Keywords:
Alphavirus
Immunology
Natural killer cells
Encephalitis
VEEV

ABSTRACT

TC83 is a human vaccine with investigational new drug status and is used as a prototype Venezuelan equine encephalitis virus for pathogenesis and antiviral research. Differing from other experimental models, the virus causes high titer infection in the brain and 90–100% mortality in the C3H/HeN murine model. To better characterize the susceptibility to disease development in C3H/HeN mice, we have analyzed the gene transcriptomes and cytokine production in the brains of infected mice. Our analysis indicated the potential importance of natural killer cells in the encephalitic disease development. This paper describes for the first time a pathogenic role for natural killer cells in VEEV encephalitis.

1. Introduction

Viruses are currently the most common cause of encephalitis. Arboviruses in the *Alphavirus* genus in the family *Togaviridae* contain multiple viruses capable of causing human encephalitis [1]. Of these, VEEV represents the most significant human pathogen. An investigational new drug (IND) vaccine strain of VEEV, TC83, is used to vaccinate at risk laboratory personnel as well as military personnel (IND No. 142) [2]. Of particular interest to this study is the unusual virulence of TC83 in C3H/HeN (C3H) mice [3,4]. Primary aerosol or intranasal infection of C3H mice with TC83 results in high levels of mortality not seen in other inbred strains [4,5]. Intranasal administration of TC83 in C3H mice closely mimics virulent VEEV encephalitis in murine models and has been used as a model to evaluate antivirals for alphavirus infection [5,6]. A clearer understanding of the host response to TC83 inoculation, given the strain's IND status, is crucial to furthering future vaccine development efforts as well as validating TC83 as the current vaccine.

Natural killer (NK) cells are one of the earliest immune effectors and in multiple models of viral infection have been implicated in control of infection through IFN-γ secretion and induction of antigen-nonspecific cell death [7,8]. They may also aid in preventing neuroinflammation [9,10]. However, the non-specific nature of NK cell action can have pathogenic effects following viral infection [7,11]. Additionally, NK cell cytokine secretion can affect the adaptive immune response, and NK cells have recently been shown to be capable of a limited memory response [12,13].

In this paper, we demonstrate for the first time that NK cells are essential for the encephalitic diseases development in C3H mice infected with TC83; however, a direct or indirect role for NK cells in host pathogenesis remains to be determined.

2. Materials and methods

2.1. Mice

The C57BL/6 mice were purchased from Jackson Laboratories (Bar Harbor, Maine). C3H/HeN mice were purchased from Charles River Laboratories (Wilmington, MA). All studies were carried out in ABSL-2 and were approved by the Institutional Animal Care and Use Committee at the University of Texas Medical Branch.

2.2. Virus challenge

Challenge with vaccine strain of VEEV (TC83) was performed as follows: at day 0, mice were challenged intranasally (i.n.) with 1×10^7 plaque forming units of VEEV (TC83) per animal in 40 μl

* Corresponding author at: 301 University Blvd Galveston, TX 77550-0609, USA. Tel.: +1 409 266 6913; fax: +1 409 747 0762.
E-mail addresses: kattaylo@utmb.edu (K. Taylor), oakoloko@utmb.edu (O. Kolokoltsova), mjpatter@utmb.edu (M. Patterson), alpoussa@utmb.edu (A. Poussard), jeksmith@utmb.edu (J. Smith), dmestes@uga.edu (D.M. Estes), slpaessl@utmb.edu (S. Paessler).

0264-410X/$ – see front matter © 2012 Elsevier Ltd. All rights reserved.
http://dx.doi.org/10.1016/j.vaccine.2012.03.076

of PBS administering approximately 20 μl per nare. Mice were observed daily.

Statistical analysis. Statistical analysis and comparison of survival for all groups over the study period was performed using log rank test at a significant level of $\alpha < 0.05$ in GraphPad® Prism (San Diego, CA).

2.3. Viral replication in the tissues

Viral replication in the brains and peripheral organs was assessed by plaque assay [39]. Mouse organs, e.g., brain, lungs, liver, spleen and kidneys, were collected at 24 h and 6 days post-challenge and sagittally sectioned in half. One half of each brain was homogenized in MEM containing 10% FBS, and a 10% suspension was made.

2.4. IVIS imaging

All imaging was performed as previously described [14].

2.5. Histopathology

Histopathology analysis of brain sections was performed by a neuropathologist blinded to the sample identification. Semi-quantitative scoring of sections was performed based on scoring system determined by trained neuropathologist. Brain sections were scored 0–3 with 0 representing no inflammation or necrosis, 1- mild/minimal inflammation (few cellular infiltrates, minimal or absent meningitis and perivascular cuffing) 2-moderate inflammation (increased cellular infiltrates, meningitis present and perivascular cuffing) 3-moderate/severe inflammation (necrosis, cellular infiltrates, diffuse meningitis, perivascular cuffing.

2.6. Microarray analysis

Microarrays quality assessment (*affy* [15], *affyPLM* [16] and *QCReport*, *affycoretools* packages), preprocessing (*gcrma* package [17]) and differential expression analysis (*limma* package [18,19]) were performed with Bioconductor software packages [20] in R programming environment [21].

Hierarchical clustering of differentially expressed genes was performed in the Spotfire Decision Site 9.0 for Functional Genomics (Spotfire Inc., Somerville, MA) using Unweighted Pair-Group with Arithmetic Mean and Euclidian distance method [22].

Differentially expressed genes were associated with biological functions and/or diseases or with canonical pathways in Ingenuity's Knowledge Base of the Ingenuity Pathways Analysis (Ingenuity Systems, http://www.ingenuity.com). Right-tailed Fisher's exact test was used to calculate a *p*-value determining the probability that the association between the genes in the dataset and the canonical pathway or biological function and/or disease is caused by chance.

2.7. Total RNA preparation and GeneChip processing

A midline saggital sections of brain was removed and DNase-treated total RNA was isolated using TRIZOL Reagent followed by the RNAqueous Mini and RNeasy-Free DNAase Set according to the protocols adapted from the manufacturer's instructions. Total RNA was subjected to GeneChip Expression Analysis (Affymetrix, Santa Clara, CA) according to the manufacturer's instructions [Expression Analysis Technical Manual, Section 2: Eukaryotic Sample and Array Processing, Alternative protocol for One-Cycle cDNA synthesis followed by synthesis of biotin-labeled cRNA with MessageAmp Premier RNA Amplification Kit (Ambion Inc., Austin, TX)] in the Molecular Genomics Core (University of Texas Medical Branch, Galveston, TX). Total fragmented cRNA was hybridized to the Affymetrix Gene Chip Mouse Genome 430A 2.0 Array using the GeneChip Hybridization Oven 640. The chips were washed and stained in a GeneChip Fluidics Station 450 and fluorescence was detected with an Affymetrix-GS3000 Gene Array scanner using the GeneChip Operating System software (GCOS1.4). The microarray data from this study can be accessed at http://www.ncbi.nlm.nih.gov/geo/, accession number.

2.8. Bioplex analyses of cytokine and chemokine expression

Brain homogenate levels of 23 cytokines and chemokines (IL-1α, IL-1β, IL-2, IL-3, IL-4, IL-5, IL-6, IL-9, IL-10, IL-12p40, IL-12p70, IL-13, IL-17, Eotaxin, G-CSF, GM-CSF, IFN-γ, KC, MCP-1, MIP-1α, MIP-1β, RANTES, and TNF-α) were determined using Bio-Plex Pro Mouse Cytokine 23-plex Assay (Bio-Rad #M60-009RDPD). Samples were collected at 24 h and/or 6 days post-infection and analyzed as per manufacturer's instructions. Replicates of two to three mice per group per time point were used.

Statistical analysis. Statistical analysis and comparison of cytokines for all groups was performed using a two-tailed unpaired Student's *t*-test with 95% confidence interval in GraphPad® Prism (San Diego, CA). In the event the *F* test to compare variance was significantly different, Student's *t*-test was used with Welch's correction.

2.9. NK cell depletion

30 μl of rabbit anti-asialo GM1 antibody (Wako Chemicals) reconstituted in 1 ml of phosphate buffered saline (PBS) was administered intraperitoneal (i.p.) prior to infection at days eight, four, and 0 and post-infection at days four, eight, and 12 unless otherwise noted. Control mice received 30 μl of polyclonal rabbit IgG at the same time point (Jackson Labs). Two NK cell depleted and two NK cell competent mice were sacrificed and spleens harvested at day 0 and day 6 to confirm NK cell depletion by flow cytometric analysis.

2.10. NK cell isolation

NK cells were isolated from donor C3H mice on day of adoptive transfer. Briefly, 20 donor spleens were removed and single cells suspensions generated by mechanical disruption. Splenocytes were fractionated over Lympholyte-M according to the manufacturer's protocol (Accurate Chemicals, Westbury, NY). The cells were washed twice in MACS buffer (phosphate buffered saline, pH 7.4 supplemented with 0.5% bovine serum albumin (BSA), 2 mM EDTA) and NK cells were separated by magnetic sorting-based negative selection according to the manufacturer's instructions (AutoMacs, Miltenyi Biotec; Auburn, CA). Purity was confirmed by cell surface staining and flow cytometric analysis.

2.11. Flow cytometric analysis

Cells (1×10^6/tube) were incubated for 10 min on ice in 50 μl blocking buffer (PBS/0.5% BSA). FITC-conjugated CD49b anti-mouse antibody (BD Pharmingen, San Jose, CA) was added (1:100) and cells incubated for 30 min at 4 °C. Cells were washed in FACS buffer and fixed in PBS/2% formaldehyde for fluorescence-activated cell sorting (FACS) analysis. Acquisition of data was performed on a FACScan flow cytometer (Becton Dickinson, San Jose, CA) and data analysis with CellQuest software (Becton Dickinson, San Jose, CA). NK cell populations were gated based on forward and side scatter and expression of CD49b. A minimum of 10,000 events were acquired for analysis. Depletion was confirmed at >90%.

2.12. Adoptive transfer

Five NK cell depleted mice were injected 24 h prior to infection via intraperitoneal (i.p.) route with 5×10^7 NK cells obtained from naïve C3H donor mice and cells were suspended in 100 μl of sterile phosphate-buffered saline (PBS). At time of transfer, 30 μl of mouse-anti-rabbit IgG was administered to mice and treatment with anti-asialo GM1 was halted (Jackson Labs). As controls for reconstitution experiments, five NK cell depleted mice were inoculated i.p. with 100 μl of PBS and 30 μl of mouse-anti-rabbit IgG. At day 0, mice were challenged as previously described.

3. Results

Previous in vivo studies demonstrated variable susceptibility of different mouse strains to TC83-induced encephalitic disease. C3H mice are highly susceptible to disease development after intranasal infection unlike other inbred strains (BALB/c and C57BL/6), which become infected but do not develop encephalitic disease [3–5]. To determine the basis for susceptibility in C3H mice, we examined the host response in the brain following intranasal infection with TC83. We found a high-titer viral load in the brain and low-titer viral load in peripheral organs at 6 dpi. In addition, pathological manifestations of disease were similar in the brain. No significant differences were observed in comparison to resistant BL6 mice . Thus, basic virology, pathology and serological methods indicated productive, robust infection of both C3H and BL6 mice.

3.1. High-levels of mortality in C3H mice, but complete survival in BL6 mice characterize intranasal TC83 infection

C3H mice had high mortality with only 10% ($n = 1$) survival rate. Mean time to death (MTD) was 9 days. All BL6 mice and sham infected mice survived infection (Fig. 1A). Both strains of mice developed symptomatic infection characterized by rapid drop in weight compared to control saline treated mice. C3H mice lost an average of 32.91 ± 6.11 percent of their body weight compared to BL6 mice that lost only 13.16 ± 5.11 percent compared to baseline body weight. Between days nine and 12, BL6 mice regained an average of 5.99 ± 4.86 percent of baseline weight indicating recovery. However, BL6 mice maintained a significantly lower weight compared to saline treated BL6 controls over the study course (Fig. 1B). Return to normal weight in TC83 infected C3H mice is due to the 10% survival rate in these mice ($n = 1$). Clinical signs of disease were more severe in C3H mice and characterized by piloerection, ataxia, severe hunching, lethargy, and hypersensitivity. BL6 mice rarely showed overt clinical signs of disease and only few mice exhibited hunching or piloerection (data not shown). Thus, both strains developed significant clinical disease, but neurological symptoms and mortality were only recorded for C3H mice.

3.2. Both C3H and BL6 mice display high-titer viral load in the brain and low-titer viral load in peripheral organs

Despite differences in mortality and disease severity, both strains had equivalent viral loads in the brain at 24 h and six days post infection indicating that level of viral replication was not a significant determinant of outcome in this model (Fig. 1C). All BL6 mice and the one remaining C3H mice cleared virus to below the limit of detection by end of study.

In order to limit the number of mice utilized, in vivo IVIS imaging was utilized to confirm the similarity in viral replication in the brain between strains. The similar viral kinetic between strains was confirmed following intranasal infection with TC83-luciferase and daily imaging for 12 days. TC83-luciferase infection results in asymptomatic, non-lethal viral invasion of the CNS. However, viral replication to a high level occurs in the brains of infected mice. Difference in signal was not significant at any time point post-infection. Bioluminescent signal directly correlates with viral load in the brain (Fig. 2A). Interestingly, three-dimensional reconstruction of bioluminescence in the brain of infected mice demonstrated

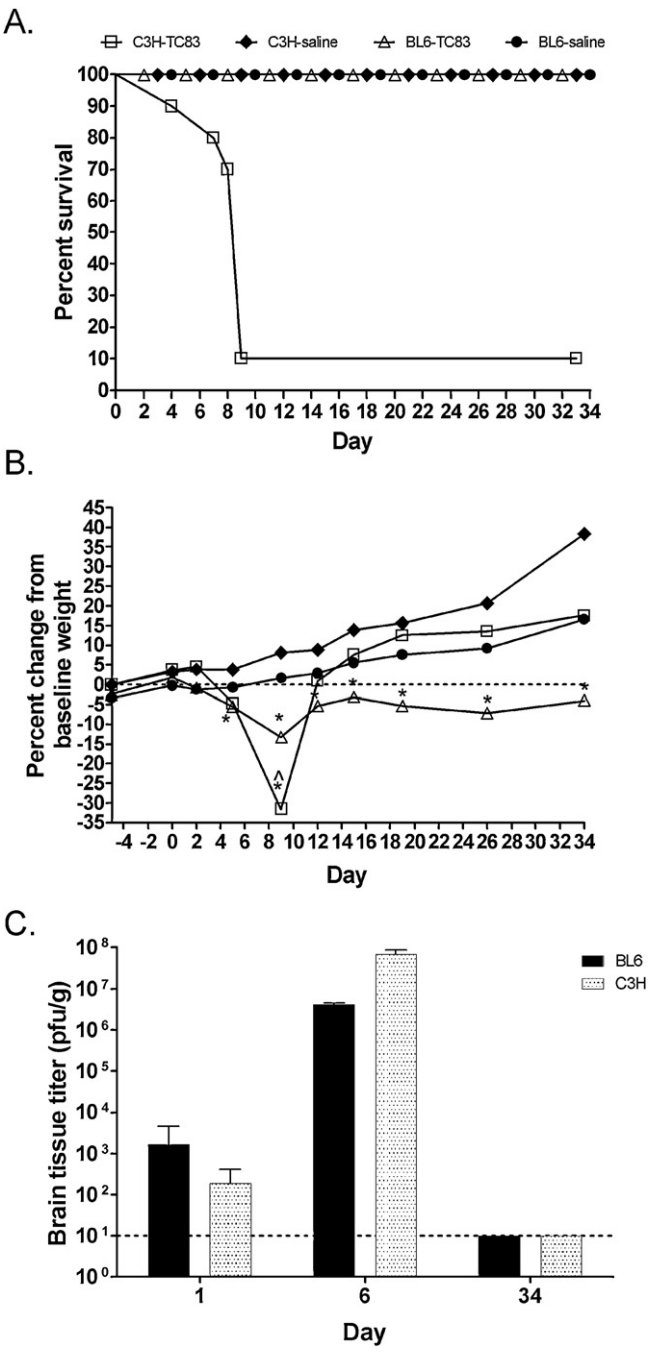

Fig. 1. Pathogenesis of intranasal TC83 infection in C3H and BL6 mice. (A) Percent survival in C3H and BL6 mice infected intranasally with TC83. Survival was significantly lower in C3H infected mice compared to BL6 infected mice. Survival was significantly lower between C3H mice compared to C3H saline treated controls ($p < 0.05$). (B) Infected C3H mice displayed significantly greater weight loss than infected BL6 mice at nine days post-infection ($p < 0.05$). Infected C3H mice lost significantly more weight than C3H saline treated controls at nine days post infection ($p < 0.0001$). BL6 mice lost significantly more weight and maintain significantly lower weights than saline controls starting at five days post-infection ($p < 0.001$). (C) Similar viral kinetic between C3H and C57 inbred mice following intranasal TC83 infection. At 24 h and six days post infection C3H mice and C57 mice have no significant difference in viral load ($P < 0.05$). At 34 days post-infection C57 mice have no infectious virus present in the brain. One surviving C3H mice had no virus present in the brain at time of termination.

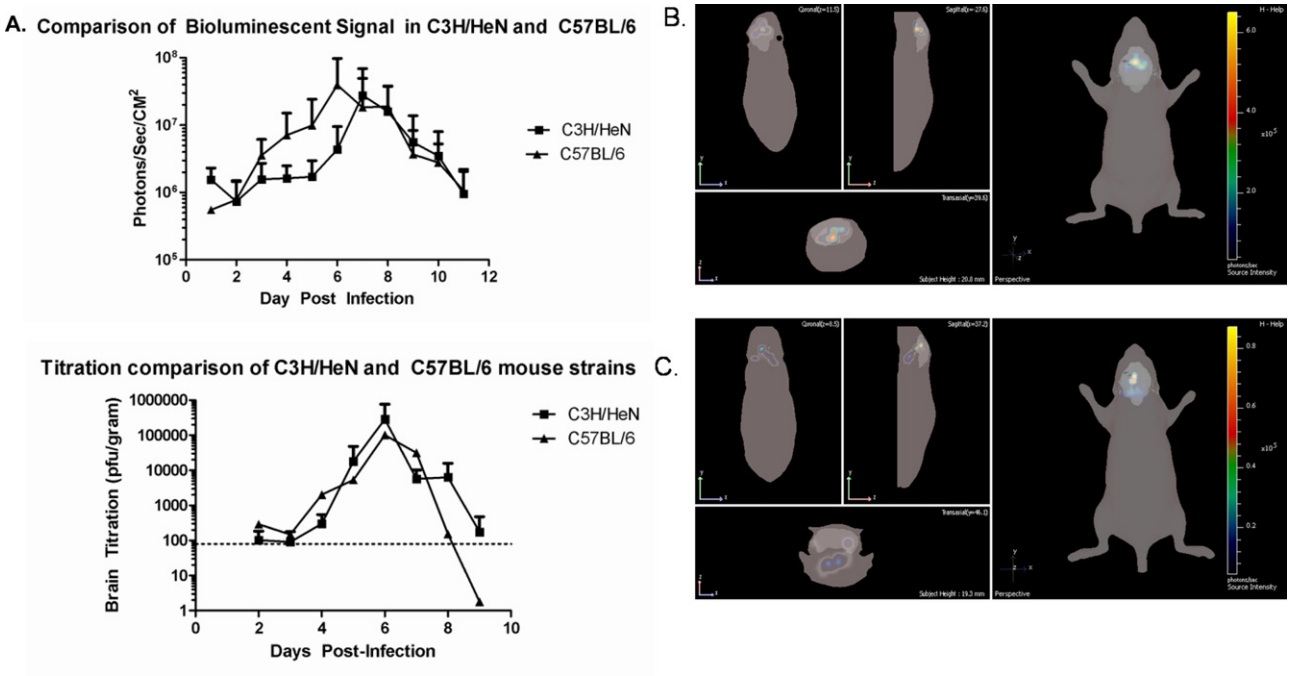

Fig. 2. Similar viral kinetic between C3H and BL6 mice. Mice were infected intranasally with attenuated TC83-luc at 10^7 plaque forming units at day 0. Bioluminescent signal in the brain was monitored for 11 days. (A) TC83-luc bioluminescent signal was not significantly different between C3H and BL6 mice at any time point post infection. Plaque assay of mice infected with TC83-luc directly correlated with bioluminescent signal. (B) Three-dimensional reconstruction of bioluminescent signal at 6 days post-infection in the brain of a representative BL6 mouse. (C) Three-dimensional reconstruction of bioluminescent signal at six days post-infection in the brain of a representative C3H mouse. More caudal spread of the virus is apparent.

alterations in spread and location of virus at the peak of acute infection in C3H and BL6 mice (Fig. 2B and C). More caudal spread is demonstrated in C3H mice (Fig. 2C). No virus was observed in peripheral organs at any time point by IVIS imaging. IVIS imaging confirmed the similarities in viral replication over time found by plaque assay with wild-type TC83 and indicated that suppression or enhancement of viral replication could not explain resistance in BL6 mice or pathogenesis in C3H mice.

Viral replication outside the CNS was not responsible for mortality either, and a similar viral load between strains at 6 dpi was observed. Viral loads in the peripheral organs (liver, lung, and spleen) were minimal and ranged from below the limit of detection to 10^3. Of the mice displaying virus at 6 dpi, C3H and BL6 mice displayed similar viral loads in the spleen of $5 \times 10^1 \pm 8.66 \times 10^1$ (1/3) and $7.5 \times 10^2 \pm 6.61 \times 10^2$ (2/3) respectively. Only 1/3 of mice demonstrated virus in the lung for both groups, and only 1/3 of C3H mice demonstrated virus in the liver, $3.33 \times 10^2 \pm 5.77 \times 10^2$ (1/3). No BL6 mice displayed virus in the liver. Viral loads for the lung in C3H mice were $3.33 \times 10^4 \pm 5.77 \times 10^1$ (1/3) and for BL6 mice were $1.67 \times 10^1 \pm 2.89 \times 10^1$ (1/3). Thus, the level of virus present over time in both the CNS and the periphery is similar between strains.

3.3. High-level production of neutralizing antibody

At six days post-infection, antibody responses were similar between infected strains with both developing equivalent levels of neutralizing antibody at six days post-infection (data not shown).

3.4. Comparative brain pathology in lethally infected C3H and resistant BL6 mice

Both strains exhibited similar histological signs of encephalitis by H&E. Increased cellular infiltrates, meningitis, and perivascular cuffing was disseminated through the brains of both strains at 6 days post infection.

3.5. Microarray analysis of brain homogenates from infected and uninfected C3H mice

To gain insight into the host response to TC83 infection, we first compared the transcriptional profiles of mock-infected mice to TC83 infected C3H mice at the peak of acute disease associated with uniform high viral load in the brain and significant clinical symptoms, six days post-infection. Transcripts with low probability values adjusted for multiple testing ($p < 0.0001$) and log2(fold change) > 1 were qualified as differentially expressed.

At six days post-infection, C3H displayed 2-fold or more differential expression of 574 genes. Infected mice had 24 genes more than 2-fold down-regulated and 550 transcripts more than 2 fold up-regulated in brain homogenates of TC83-infected compared to mock-infected C3H mice.

Functional analysis was performed on differentially expressed genes through association with specific biological functions and disease. Differentially expressed genes involved several overlapping categories related to immune and inflammatory function (antigen presentation, cell and humoral immunity, and inflammatory response) in the brain homogenates of infected mice compared to sham infected mice. A number of these genes in immune and inflammatory functional categories also overlapped with canonical pathways associated with cell death. More than 83% (192/229) of genes differentially expressed two-fold or greater in immune/inflammatory functioning overlapped with genes involved cell death. Unsurprisingly, these immune response transcripts were largely involved in recognition of viral pathogens and interferon signaling, typical for alphaviral infections (Fig. 3A). However, multiple genes involved in signal transduction between natural killer cells and antigen presenting cells

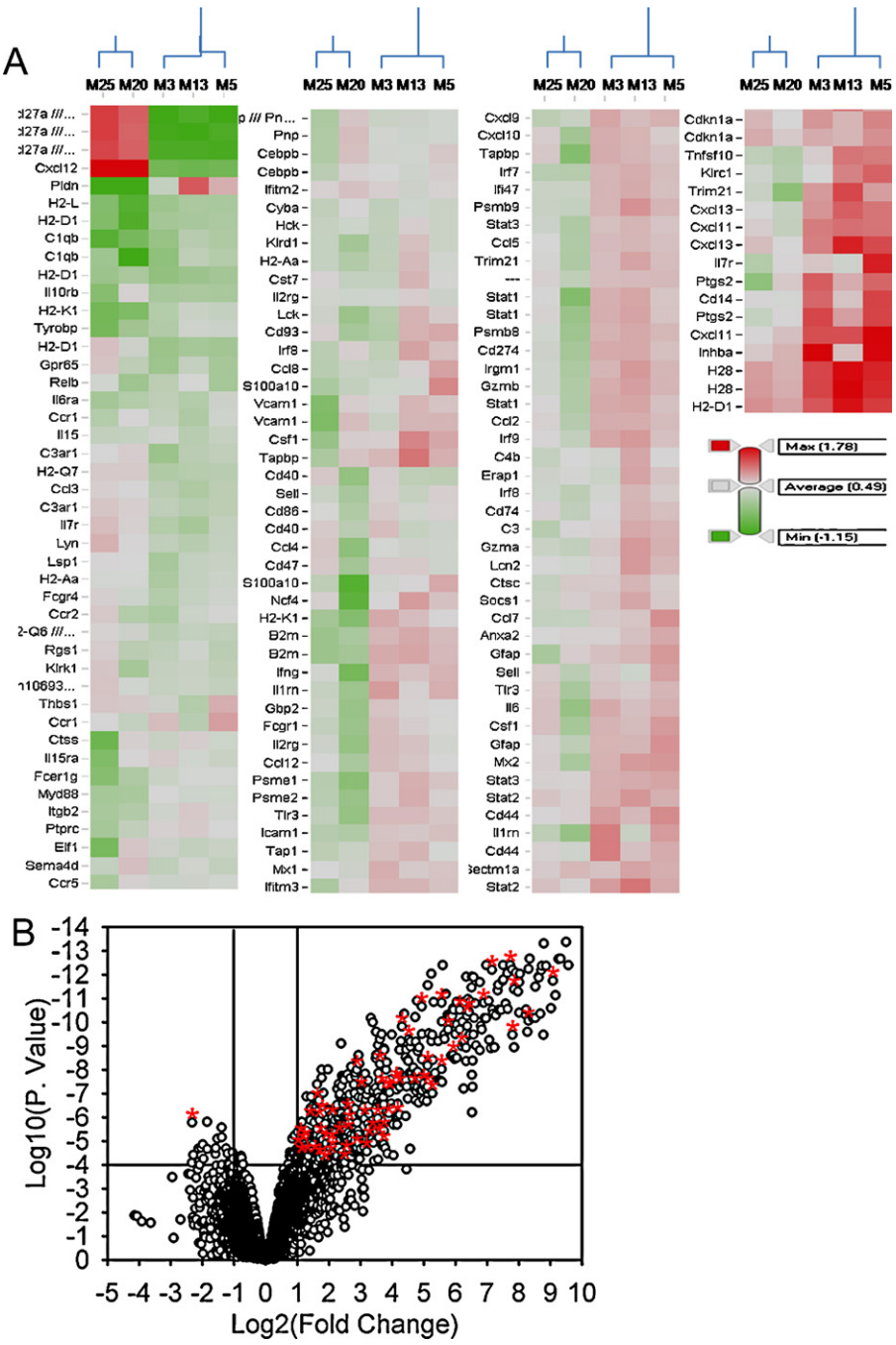

Fig. 3. Alterations in immune/inflammatory response upon intranasal infection of C3H mice with TC83 virus. (A) Heat map plot of differentially expressed immune/inflammatory transcripts (from functional categories representing antigen presentation, cell-mediated immune response, humoral immune response, and inflammatory response) for C3H infected mice. Rows are arranged by hierarchical clustering following *Z*-score transformation of the normalized data. Columns represent mock-infected and TC83-infected mice at six days post-infection. Rows are arranged by hierarchical clustering following *Z*-score transformation of the normalized data. Columns represent mock-infected C3H (M25 and M20), TC83-infected C3H(M3, M13, and M5), transcripts from brain homgenates at 6 days post challenge. (B) Volcano plots of microarray results with identification of differentially expressed natural killer cell related gene transcripts represented by red (upregulated) and green (downregulated) circles. Gene expression was compared between C3H and saline C3H samples at six days post-infection. The horizontal line represents significance ($p < 0.0005$) and the vertical lines represent the change in gene expression for C3H mice compared to that for C3H-saline mice [Log2(fold change) > 1]. (For interpretation of the references to color in the figure caption, the reader is referred to the web version of the article.)

were also demonstrated (CCL13, CCL2, CCL4, CCL5, CCL7, CCR1, CCR2, CCR5, CD14, CD274, CD40, CD44, CD47, CD52, CD72, CD74, CD86, COL4A1, COL4A1, CSF2RB, CXCL10, CXCL12, CXCL9, FCER1G, FCGR1A, FCGR3A, FGL2, GZMB, H2-Id, H2-Q5, H2-T10/H2-T22, HBEGF, HCK, HLA-B, HLA-C, HLA-DQA1, HLA-DQA1, HLA-G, IFNG, IGFBP7, IL13RA1, IL15, IL15RA, IL1RN, IL1RN, IL2RG, IL2RG, IL6, IL6R, IL7R, IL7R, KLRC1, KLRD1, KLRK1, LYN, TLR3, TNFSF10, TYROBP) (Fig. 3B, Table 1). The more than two-fold differential expression of non-classical MHC class I genes (H2-LD, H2-Q5, H2-T10, HLA-B, HLA-C, HLA-DQA1, HLA-E, HLA-G) between C3H and saline control mice was important given the limited expression of classical MHC I expression in the brain making non-classical MHCI essential in regulation of the immune response in the microenvironment of the brain. In addition, greater than two-fold up-regulated expression of *H2-Q5* was found in TC83-infected C3H mice. Isoforms of H2-Q5 are enriched in the brain and encode a Qdm leader peptide. Qdm can

Table 1
Genes involved in signal transduction between natural killer cells and antigen presenting cells.

Symbol	Fold change	*p*-Value
CXCL12	−5	1.65E−06
CD47	2	2.01E−05
COL4A1	2.2	6.72E−06
CCR1	2.2	4.33E−05
CD40	2.3	1.32E−05
HBEGF	2.3	9.52E−06
IL6R	2.5	0.000041
LYN	2.6	1.23E−06
COL4A1	3	3.71E−05
IL15	3.1	2.22E−07
CD40	3.3	1.33E−06
IGFBP7	3.3	5.21E−05
IL13RA1	3.3	6.51E−06
KLRK1	3.4	7.15E−07
TNFSF10	3.5	7.31E−07
IL13RA1	3.6	8.64E−05
IL15RA	3.8	1.23E−05
CSF2RB	4.2	4.42E−05
IL7R	4.3	1.17E−05
CD44	4.3	1.07E−06
HBEGF	4.3	2.66E−05
CCL4	5	6.13E−06
IL7R	5.6	7.93E−05
IL13RA1	5.9	3.45E−05
CD14	6.1	6.15E−07
HLA-C	6.1	4.46E−06
KLRD1	6.2	1.76E−06
CCR1	7.4	1.82E−05
H2-Q5	7.4	9.86E−09
HLA-C	8.1	7.31E−08
IL1RN	8.8	1.13E−06
HLA-DQA1	9.1	2.71E−05
CCR2	9.7	8.58E−06
TYROBP	10.4	3.98E−06
CCR5	11.6	1.10E−06
HLA-DQA1	11.9	7.09E−06
TLR3	12.2	5.66E−09
HCK	12.7	5.14E−08
KLRC1	13.3	1.38E−05
CD72	13.4	3.62E−06
HLA-G	13.9	7.72E−08
IFNG	14.8	1.01E−06
IL6	14.9	8.41E−08
CD74	15.1	9.03E−08
IL2RG	17.3	4.20E−08
CD86	17.5	3.11E−08
FCGR3A	18	8.81E−07
HLA-B	18.8	5.27E−08
TLR3	19.8	1.52E−10
H2-Id	22.9	5.23E−10
CCL7	26	5.14E−08
HLA-C	30.5	2.18E−11
HLA-C	32	3.68E−08
FCER1G	34.6	5.14E−08
HLA-B	34.6	6.63E−09
FGL2	38.5	9.77E−08
H2-T10/H2-T22	47.2	1.51E−11
CD44	47.2	9.38E−09
CD52	54.4	2.03E−10
IL1RN	60.7	2.41E−09
HLA-C	70.1	3.00E−11
HLA-C	73.4	1.01E−09
CCL13	82.3	5.41E−11
IL2RG	85.9	3.65E−11
FCGR1A	117.9	1.51E−11
CCL2	142	6.21E−13
CD274	212	3.95E−13
CXCL9	222.7	3.40E−10
CCL5	230.7	4.06E−12
GZMB	316	8.63E−11
CXCL10	539.7	1.79E−12

be donated to Qa-1 and act in an inhibitory role on CD94/NKG2A positive cytotoxic cells [30]. These factors indicated that control of natural killer cell populations was a significant component of TC83 infection in C3H mice (Fig. 3B).

3.6. Cytokine expression patterns indicate NK cell involvement in C3H susceptibility

Levels of IL-2, an important factor in NK cell development and maintenance, are lower than control mice at 24 h post-infection but significantly higher at 6 days post-infection. The relationship over time in IL-2 levels in the brain indicates significant differences in maintenance and activation of NK cell populations in the brain between C3H and saline C3H mice (Fig. 4). At six days following infection, both KC levels and MCP-1 levels in the brains of C3H mice are significantly higher than controls (Fig. 5). MCP-1 is an important factor enhancing NK cells and other monocytic infiltration to the CNS [23]. IL-12p40 levels are also significantly elevated in both strains (Fig. 5). The balance between IL-12p40 and other inflammatory cytokines or chemokines, particularly MCP-1, has been shown in other models to be related to outcome to infection [24,25]. Thus, while active monocytic recruitment and activation occurs in both strains, the phenotypic differences in cytokine expression indicate differential activation and recruitment of specific cell populations.

C3H mice display significant differences in IL-1β, IL-5, MIP1β, and RANTES when compared to saline controls (Fig. 5, data not shown). In addition, C3H mice display significant differences in IL-1α, IL-3, IL-6, IL-10, IL-12p70, IL-17, eotaxin, and G-CSF compared to saline control mice at six days post-infection.

MCP-1 levels at six days post-infection are corroborated by microarray assay where levels of *ccl3* and *ccl13* are more than 2-fold increased in infected mice compared to saline controls. Further, MIP1β, IL-6, and RANTES (*ccl3*, *IL-6*, *ccl5*) transcripts are more than two-fold upregulated in C3H mice compared to controls. Additionally, the receptor transcripts for IL-2, IL-6, IL-3, IL-10, IL-17 (*IL-2RG*, *IL-6R*, *CSF2RB*, *IL-10RB*, *IL17RA*) are all 2-fold greater than saline controls.

Thus, despite a trend toward a robust pro-inflammatory response in C3H mice, significant production differences in a subset of cytokines indicates alterations in recruitment, maintenance, and regulation of specific cell populations, particularly natural killer cells, between infected and uninfected mice.

3.7. Depletion of NK cells reverses the infection outcome in C3H mice

In order to examine the role of NK cells in TC83-encephalitis, we utilized the common technique of anti-asialo GM1 administration to deplete NK cells from C3H mice prior to and during infection [26].

A reversion of disease outcome was observed following depletion. NK cell-depleted mice had survival rates of 80–100% depending on trial compared to complete mortality in wild-type mice. An initial pilot study demonstrated that depletion of NK cells from immunocompetent C3H/HeN mice ($n = 3$) resulted in 100% survival compared to uniform mortality in undepleted control mice who had a mean day to death of eight days ($n = 5$) ($p = 0.0082$). Survival to saline controls could not be determined ($n = 1$). NK cells were depleted by i.p. administration of anti-asialo-GM1 antibody prior to infection and throughout the course of infection. A repeated study to confirm findings demonstrated 80% survival in infected NK cell depleted mice ($n = 10$) and represented a significant increase over complete mortality observed in NK cell competent infected mice who had a mean day to death of nine days ($n = 10$) ($p < 0.0001$) (Fig. 6A). Congruent with survival, mice depleted of NK cells lost significantly less weight than NK cell competent infected positive

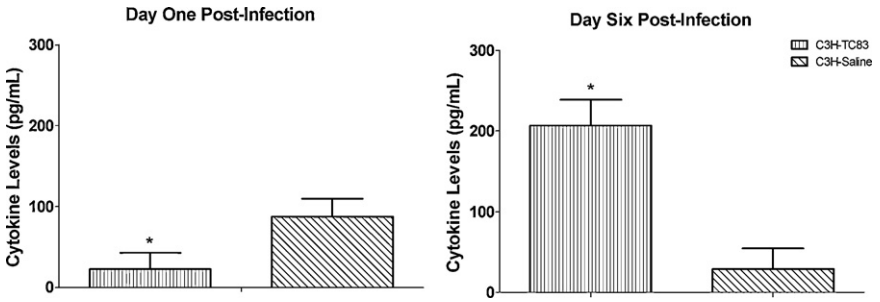

Fig. 4. Inverse patterns of IL-2 expression over time in the brain during the course of infection in saline and TC83-infected C3H. Lethally infected C3H mice demonstrate significantly lower levels of IL-2 at one day post-infection, but at six days post-infection have significantly higher levels of IL-2 compared to saline treated C3H mice ($^{*}p < 0.05$; $^{**}p < 0.005$).

controls in both trials. However, NK cell depleted mice still developed symptomatic disease losing significantly more weight than sham infected depleted mice without developing neurological disease. Between days nine and 17 in the second trial, NK cell depleted mice regained a large percentage of body weight indicating recovery. Treatment with anti-asialo GM-1 antibody alone did not result in clinical symptoms or weight loss compared to mice treated with control rabbit IgG (Fig. 6B).

Thus, NK cell depletion of C3H mice following TC83 infection results in complete protection against lethal encephalitis.

3.8. NK cells increase viral burden in the host

By examining viral replication, histological manifestations of encephalitis and cytokine profiles of lethally infected wild-type C3H and surviving NK cell depleted mice, we hoped to gain insight into the mechanism of NK cell action in the brain following TC83-encephalitis. While a high-titer viral load resulted in both NK cell depleted and wild-type mice, viral load in the brain was slightly reduced by NK cell depletion at six days post-infection in the second trial. At day eight post-infection in the first trial, no significant difference was observed (Fig. 6C). While no difference in viral load was noted in the brain at 24 h post-infection, peripheral organ viral titers (liver, lung, and spleen) demonstrated a trend toward lower viral load at one day post-infection following NK cell depletion. C3H depleted lung viral load was $2.5 \times 10^4 \pm 2.18 \times 10^4$ (2/3) while wild-type mice were $1.47 \times 10^5 \pm 6.25 \times 10^4$ (3/3). Likewise, depleted mice liver viral loads were 0 ± 0 (0/3) while wild-type mice were $1.6 \times 10^4 \pm 1.98 \times 10^4$ (2/3). Spleen viral loads for depleted mice were also lower, $1.25 \times 10^2 \pm 2.17 \times 10^2$ (1/3) compared to wild-type mice, $5 \times 10^4 \pm 2.94 \times 10^4$ (1/3). By six days post-infection, virus was below the limit of detection (100 pfu) for all tested samples ($n = 3$/group) in this experiment. Virus was not present in the brains or peripheral organs of saline controls.

Thus, NK cell depletion appears to have a limited impact on viral load but a significant one on survival.

3.9. NK cell depleted and TC83 infected mice develop lethal encephalitis following adoptive transfer of naïve NK cells

In order to confirm the pathogenic role of natural killer cells, we performed a gain-of-function experiment supplementing NK cell depleted C3H mice with naïve NK cells prior to infection.

In order to successfully transfer NK cells into depleted mice, treatment with anti-asialo GM1 antibody was altered from previous trial and halted 24 h prior to infection and counteracted with mouse anti-rabbit IgG administration. This resulted in a change in survival rates in NK cell depleted mice dropping 40%. However, in mice given the same treatment and 10^7 naïve natural killer cells, mortality increased to 100%. This was a significant difference between groups ($p = 0.0495$) (Fig. 7A). Symptomatic disease was also similar in these mice with weight loss equivalent to that seen in infected, wild-type mice (Fig. 7B). Thus, adoptive transfer of naïve NK cells to NK cell depleted mice 24 h prior to infection results in reversion of disease phenotype to that seen in wild-type C3H mice and complete mortality by day 8.

3.10. NK cells do not affect quantitative inflammation in the brain

Histological examination of brain tissue by H&E demonstrated similarities between infected depleted and competent mice. Both survivors (NK cell depleted) and lethally infected mice (NK cell competent) have extensive signs of inflammation throughout the brain tissue with diffuse meningitis, increased cellular infiltrates, and extensive perivascular cuffing (Table 2). However, despite robust pathologies in the CNS NK cell depleted mice still survive infection.

3.11. NK cell depletion alters the host response

Despite similar pathologies, the host response was significantly altered in NK cell depleted mice compared to competent controls at both 24 h and 6 days post-infection. At 24 h post-infection, IL-12p40, a proinflammatory cytokine involved in multiple immune functions, was significantly elevated in infected wild-type mice that were not depleted of NK cells compared to infected depleted mice. Infected wild-type mice also had significantly elevated IL-12p40 levels when compared saline infected wild-type controls. However, NK cell depleted mice showed no difference in IL-12p40 levels compared to saline-infected depleted controls. Thus, the pro-inflammatory response appears to be significantly modified following NK cell depletion. Furthermore at 24 h post-infection, both RANTES and G-CSF levels are unchanged in NK cell depleted mice compared to controls while NK cell competent mice have significant elevation of both these cytokines. Thus, early, acute elevation in G-CSF, RANTES and IL-12p40 act as a marker for mortality

Table 2
Histological scores of brain tissue from NK cell depleted and NK cell competent C3H mice following intranasal TC83 infection at 6 dpi.

Group	*n*	Hippocampus	Thalamus	Cerebral cortex	Olfactory bulb	Cerebellum	Striatum	Meninges	Overall score
−NK	3	1 ± 0	1 ± 0	1.67 ± 0.58	1 ± 1.41	0 ± 0	1.33 ± 0.58	1.67 ± 0.58	7 ± 1
+NK	3	1 ± 0	1.67 ± 0.58	2 ± 1	1	0 ± 0	1.33 ± 0.58	1.33 ± 0.58	7.67 ± 2.08

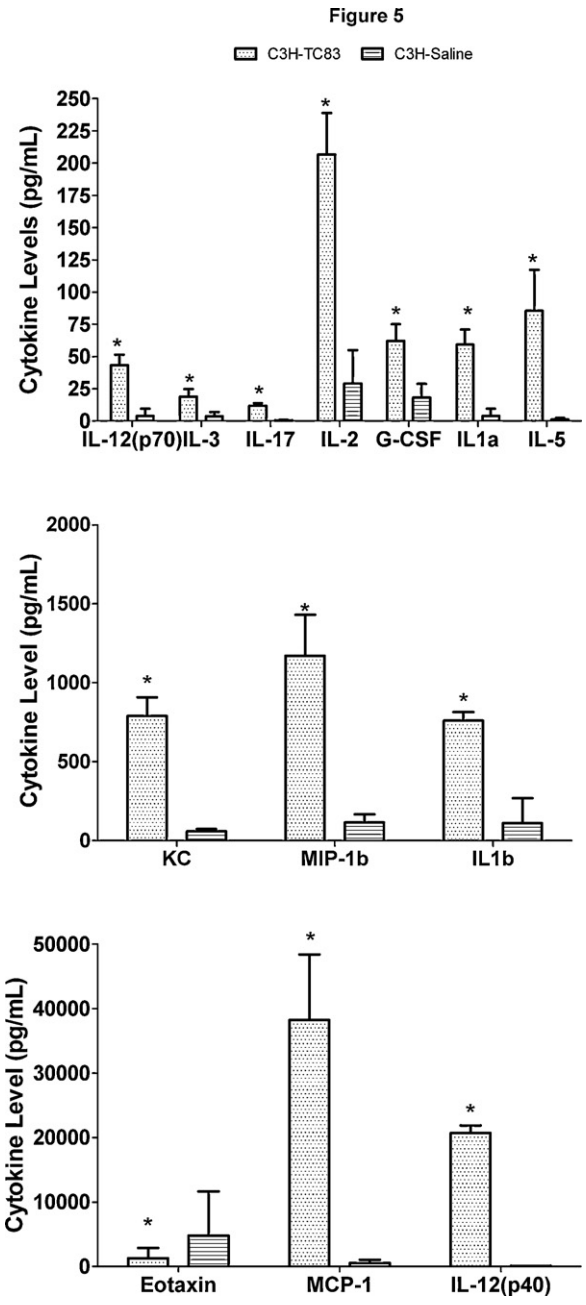

Fig. 5. Unique cytokines expression profiles in C3H infected mice compared to saline controls at six days post infection. C3H mice display significant differences in MCP-1, KC, IL-12p40, MIP-1a, IL-1b, IL-4, IL-10, G-CSF, IL-1β, IL6, IL-12p70, IL-3, and IL-17 compared to saline treated control C3H mice. No significant differences in IFN-γ expression were observed between groups though infected mice, C3H and BL6, show a trend to increased IFN-γ expression ($P < 0.05$).

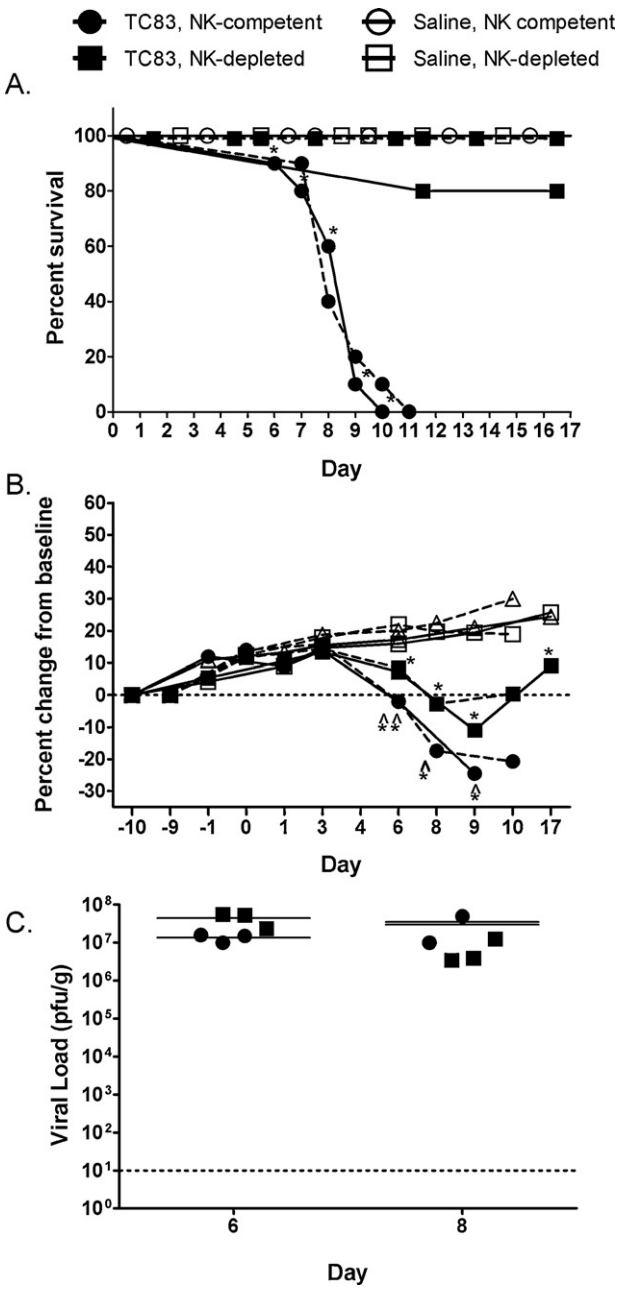

Fig. 6. NK cell depletion reverses the outcome of the infection in C3H mice. Dashed line represents separate experiment. (A) Depletion of NK cells from immunocompetent C3H mice resulted in 80–100% survival compared to uniform mortality in undepleted control mice in one experiment ($p = 0.0082$). (B) Mice with NK cells lost more weight compared to infected NK cell depleted mice at six and eight days post infection. For both infected groups (NK cell depleted and NK cell competent) weight loss was significantly greater compared to saline controls at both six and eight days post-infection. (C) Viral load in the brain did not differ between NK cell depleted and competent mice at eight days post-infection. In second experiment, survival of NK-depleted mice was 80%. Survival was significantly decreased in positive controls that maintained NK cells ($n = 10$) compared to infected, NK cell depleted mice ($n = 10$). (A) There was no significant difference in survival between NK cell depleted, infected mice ($n = 10$) and saline, depleted controls ($n = 4$). Survival in NK cell competent infected mice ($n = 10$) was significantly less than saline controls ($n = 4$) ($p < 0.005$). (B) Weight loss was significantly more in infected NK cell competent mice compared to NK cell depleted mice at six and nine days post-infection. NK cell depleted and competent infected mice lost significantly more weight than controls ($p < 0.005$). (C) Viral load in the braid was significantly decreased in NK cell depleted mice compared to NK cell competent mice at six days post-infection ($p = 0.0422$).

in this model. IFN-γ levels remained the same at this time point though NK cell depleted mice showed a trend towards elevated IFN-γ compared to competent infected or sham infected controls (Fig. 8).

At six days post-infection, the host response remains altered. However, an overall robust pro-inflammatory response is evidenced in both competent and depleted mice. IL-1α, IL-3, IL-4, IL-5, IL-9, IL-10, IL-13, IL-12p70, eotaxin, MIP1α, MIP1β, GM-CSF, IFN-γ, and RANTES levels in NK cell competent mice are significantly elevated compared to controls whereas only IL-1α, IL-9, IL-10, IL-13, GM-CSF, IFN-γ, MIP1α, MIP1β, and RANTES are significantly elevated in resistant NK cell depleted mice compared to saline controls

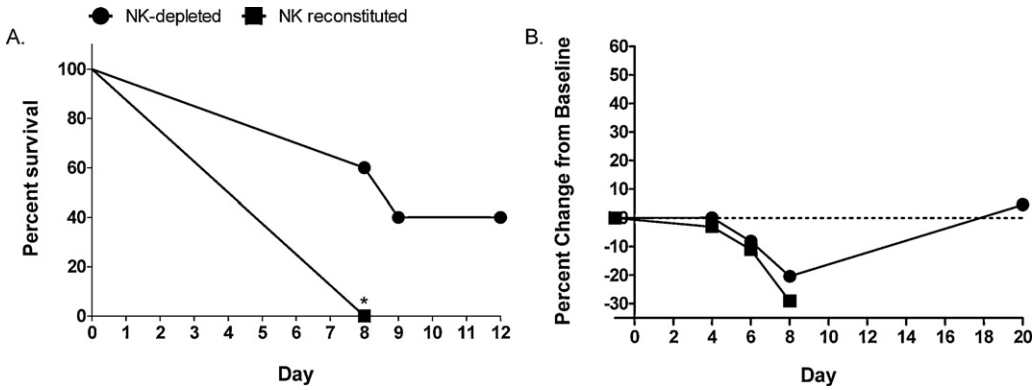

Fig. 7. Pathogenesis resulting from reconstitution of naïve NK cell cells in previously resistant NK cell depleted C3H mice. Treatment with anti-asialo GM1 antibody was halted 24 h prior to infection and counteracted with treatment with mouse anti-rabbit IgG. Mice received either 10^7 naïve NK cells or an equivalent amount of saline i.p. 24 h prior to infection. (A) Reconstitution of depleted mice with purified, naïve NK cells reverted disease phenotype to uniform mortality. This was significantly different than NK cell depleted mice that did not receive NK cells. This group had a 40% survival rate ($p = 0.0495$). (B) Weight loss was not significantly different between groups at any time point post infection. Surviving NK cell depleted mice showed weight gain indicative of survival between day eight post infection and termination of study.

(Fig. 8, data not shown). Interestingly, NK cell depletion also induces significantly higher levels of TNF-α than saline controls; NK cell competent mice display no significant change in TNF-α levels compared to saline controls. NK cell depletion induces a cytokine profile with reduced production of IL-2, IL-3, IL-4, IL-12p70, and eotaxin at day six post-infection inducing a distinct profile in these surviving mice (Fig. 8). Thus, these cytokines might provide a useful indicator of mortality and opens the possibility for different cytokines in treatment and identification of viral encephalitis.

4. Discussion

Human vaccine strain of VEEV (TC83) replicates to high levels in brains of C3H and BL6 mice. Furthermore, vaccination with TC83 is associated with poor levels of seroconversion and high numbers of adverse events in humans [27].

Current literature supports lethal intranasal infection of TC83 in C3H mice as a model to evaluate antivirals against VEEV, however, no data is available that would help explain why C3H mice develop lethal disease while other strains do not [5,6].

The results of these experiments show that qualitative differences in the host response characterizing lethal infection are able to indicate components of the immune system responsible for neuroprotection or pathogenesis during VEEV-like encephalitis. In our studies saline-treatment of C3H mice was associated with different transcriptome and cytokine profiles than lethally infected C3H mice and indicated a potential role for natural killer cells in pathogenesis. Previous studies of viral pathogenesis following aerosol infection with TC83 suggested that reduced cellular immune response in C3H mice might explain the decrease in rate of clearance compared to BALB/c mice though areas of the brain affected by viral antigen were similar [3,4]. However, no work had been performed to evaluate the specific changes in host response required for altered pathogenesis or to examine the correlates of susceptibility to TC83 challenge.

Thus, this study, through transcriptome and cytokine profiles, clearly indicated differences in the host response in the brain of infected vs. uninfected mice. Transcriptome analysis revealed changes in the robust immune pro-inflammatory response in C3H mice at the peak of acute infection. For the early host response capable of initial defense and later modulation of an effective adaptive response, only production of type I interferon (IFN) has a well defined role in VEEV-encephalitis [5,28–30]. Type I interferon (IFN), IFN-alpha and IFN-beta, production is important early in infection as evidenced by prophylactic, but not therapeutic protection. [5]. IFN also plays an important role in NK cell and adaptive immune response activation [12,13,31]. A later adaptive immune response associated with a protective phenotype to VEEV has been primarily characterized by neutralizing antibody production and generation of IFN-γ secreting $CD4^+$ T-cells [32,33].

The differential expression of genes involved in control of natural killer cells indicate the importance of appropriate modulation of the immune system in the response of C3H mice to TC83 infection [34]. Later elevation of IL-2 in lethally infected C3H mice indirectly related to NK cell activation. Along with a later increase in IL-2 levels, KC, IL-12p40, and MCP-1 levels are elevated at the peak of acute infection in lethally infected mice indicative of robust recruitment of monocytes. Combined with gene profiles and existing literature, this strongly suggested natural killer cells as a primary effector cell population in TC83-encephaltis [35–37].

A major finding of this study was a novel role for natural killer cells in the pathogenesis of encephalitis in C3H mice. Interestingly, depletion of this cell population resulted in a minimal but statistically significant suppression of viral replication at day six post-infection, possibly indicative of more rapid clearance as seen in BL6 mice.

The mechanism of NK cell induced pathogenesis remains to be determined. NK cells may be acting directly through cell to cell interactions and cellular cytotoxicity as demonstrated for Semliki Forest virus [38]. NK cells may also indirectly affect the environment of the brain through cytokine secretion. Alternatively, the phenotype and cell-to cell interactions of NK cells may be altered by specific strain of mouse either through changes in H2 alleles altering cytotoxicity or by generation of different phenotypes via altered cytokine secretion patterns. Cytokines indicative of type I IFN production were produced in C3H mice as well as in C3H depleted mice. Given the importance of type I IFN in both resistance to alphavirus infection as well as activation and determination of phenotype for NK cells, the pathogenesis of NK cell populations in C3H mice may be linked to type I IFN. However, when BL6 mice are infected with wild type VEEV (ZPC738) no changes in mortality occur between NK cell depleted and undepleted mice (data not shown) indicating that the pathogenic effect of NK-cells might be specific to C3H mice We are currently testing these hypotheses.

In summary, these studies provide a unique profile of the host response demonstrating correlates of both a protective and pathogenic host response in the CNS to viral encephalitis. Additionally, a unique role for NK cells in the pathogenesis of TC83-encephalitis was shown for the first time. Nevertheless, the precise

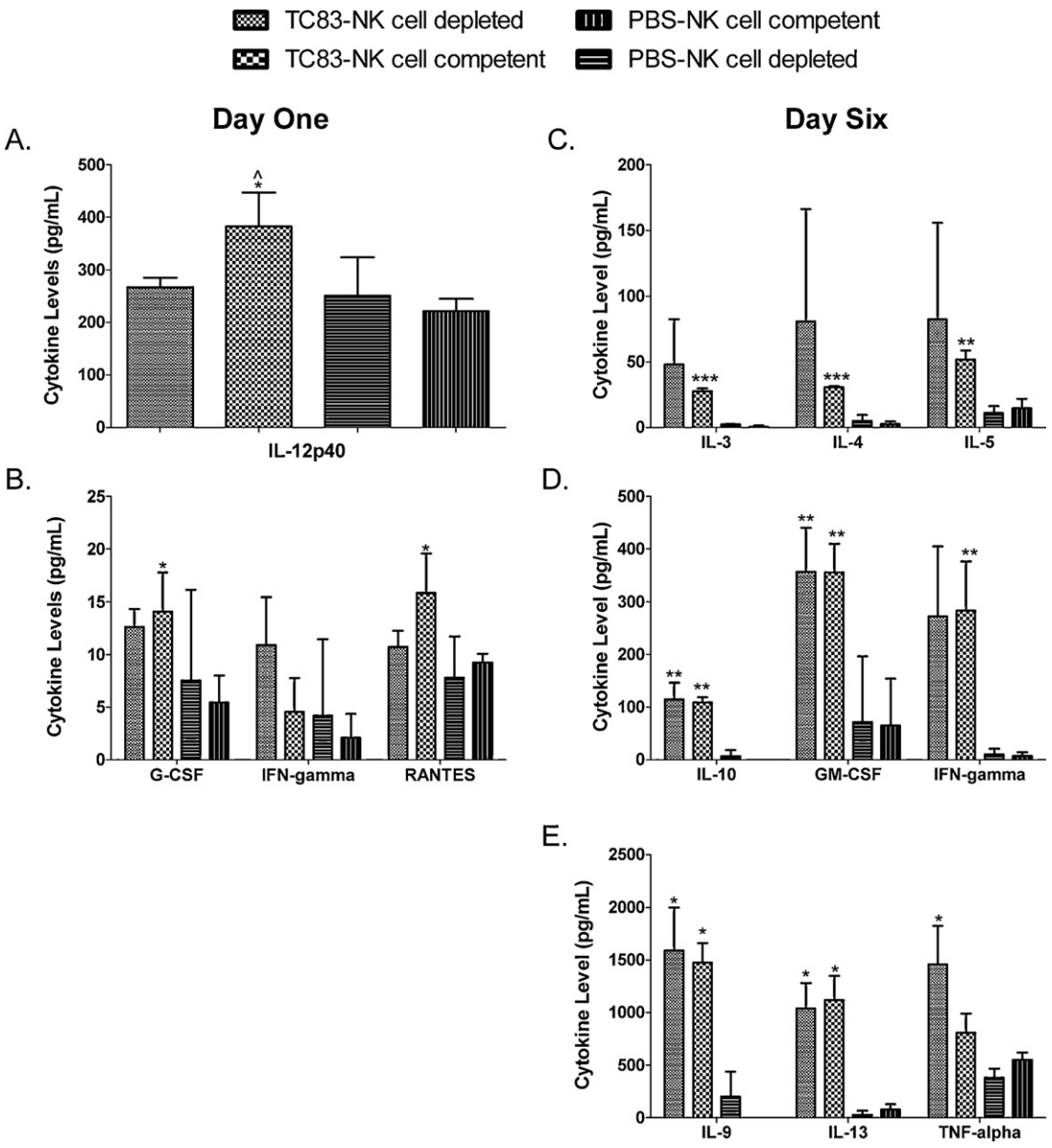

Fig. 8. Alterations in pro-inflammatory cytokine profiles from the brain homogenates of NK cell competent and NK cell depleted mice at 24 h and six days post-infection. (A and B) At 24 h post-infection, in infected mice receiving control IgG, IL-12p40, G-CSF and RANTES levels are significantly elevated above that of saline treated controls receiving control IgG (*$p < 0.05$). (A) IL-12p40 levels were significantly different between infected NK cell depleted mice that survive and lethally infected NK cell competent mice (^$p = 0.05$). (B) No significant difference in IFN-gamma levels was observed at 24 h post-infection for any group comparison. There are no significant differences between saline treated NK cell depleted and NK cell competent mice. TC83 infected mice compared to controls (*$p < 0.005$). (C) At six days post-infection, NK cell competent TC83 infected mice display significantly elevated levels of IL-3, IL-4, and IL-5 cytokines compared to NK cell competent, saline infected mice. Significant differences were not noted between NK cell depleted sham and infected mice though a trend toward increased expression in infected mice appears. No significant differences between TC83 infected NK cell competent and depleted mice were noted though all three cytokines appear to be more elevated in NK cell depleted mice. (D) IL-10, GM-CSF, and IFN-g levels are elevated in infected mice regardless of NK cell status. IFN-g levels are similar between lethally infected mice and NK cell depleted mice. (E) IL-9, IL-13, and TNF-α levels are elevated in TC83 infected mice compared to controls (*$p < 0.005$).

mode of action NK cells utilize to induce pathogenesis in the brain of C3H mice is currently unknown and under investigation.

Acknowledgements

This project was funded through Institute for Human Infections and Immunity at UTMB, Sealy Center for Vaccine Development at UTMB, and the Foreign Animal and Zoonotic Disease Center of Excellence by a grant from the Department of Homeland Security, Science and Technology Directorate, Office of University Programs. Michael Patterson was supported in part by the Institute for Translational Sciences UTMB-NIH grant 1UL1RR029876-01.

References

[1] Griffin DE. Alphaviruses. In: Knipe DMHP, editor. Fields virology. 5th ed. Philadelphia: Wolters Kluwer Health/Lippincott Williams & Wilkins; 2007. p. 1023–54.
[2] Pittman PR, Makuch RS, Mangiafico JA, Cannon TL, Gibbs PH. Long-term duration of detectable neutralizing antibodies after administration of live-attenuated VEE vaccine and following booster vaccination with inactivated VEE vaccine. Vaccine 1996;14:337.
[3] Hart MK, Pratt W, Panelo F, Tammariello R, Dertzbaugh M. Venezuelan equine encephalitis virus vaccines induce mucosal IgA responses and protection from airborne infection in BALB/c, but not C3H/HeN mice. Vaccine 1997;15(March (4)):363–9.
[4] Steele KE, Davis KJ, Stephan K, Kell W, Vogel P, Hart MK. Comparative neurovirulence and tissue tropism of wild-type and attenuated strains of Venezuelan

equine encephalitis virus administered by aerosol in C3H/HeN and BALB/c mice. Veterinary Pathology 1998;35(September (5)):386–97.
[5] Julander JG, Skirpstunas R, Siddharthan V, Shafer K, Hoopes JD, Smee DF, et al. C3H/HeN mouse model for the evaluation of antiviral agents for the treatment of Venezuelan equine encephalitis virus infection. Antiviral Research 2008;78(June (3)):230–41.
[6] Julander JG, Bowen RA, Rao JR, Day C, Shafer K, Smee DF, et al. Treatment of Venezuelan equine encephalitis virus infection with (−)-carbodine. Antiviral Research 2008;80(December (3)):309–15.
[7] Brandstadter JD, Yang Y. Natural killer cell responses to viral infection. Journal of Innate Immunity 2011;3(3):274–9.
[8] Trifilo MJ, Montalto-Morrison C, Stiles LN, Hurst KR, Hardison JL, Manning JE, et al. CXC chemokine ligand 10 controls viral infection in the central nervous system: evidence for a role in innate immune response through recruitment and activation of natural killer cells. Journal of Virology 2004;78(January (2)):585–94.
[9] Segal BM. The role of natural killer cells in curbing neuroinflammation. Journal of Neuroimmunology 2007;191(November (1–2)):2–7.
[10] Hao J, Liu R, Piao W, Zhou Q, Vollmer TL, Campagnolo DI, et al. Central nervous system (CNS)-resident natural killer cells suppress Th17 responses and CNS autoimmune pathology. Journal of Experimental Medicine 2010;207(August (9)):1907–21.
[11] Hansen DS, Bernard NJ, Nie CQ, Schofield L. NK cells stimulate recruitment of CXCR3+ T cells to the brain during *Plasmodium berghei*-mediated cerebral malaria. Journal of Immunology 2007;178(May (9)):5779–88.
[12] Sun JC, Beilke JN, Lanier LL. Adaptive immune features of natural killer cells. Nature 2009;457(January (7229)):557–61.
[13] Sun JC, Lanier LL. Natural killer cells remember: an evolutionary bridge between innate and adaptive immunity? European Journal of Immunology 2009;39(August (8)):2059–64.
[14] Patterson M, Poussard A, Taylor K, Seregin A, Smith J, Peng B-H, et al. Rapid, non-invasive imaging of alphaviral brain infection: Reducing animal numbers and morbidity to identify efficacy of potential vaccines and antivirals. Vaccine 2011;50:9345–51.
[15] Gautier L, Cope L, Bolstad BM, Irizarry RA. affy – analysis of Affymetrix GeneChip data at the probe level. Bioinformatics (Oxford, England) 2004;20(February (3)):307–15.
[16] Irizarry RA, Hobbs B, Collin F, Beazer-Barclay YD, Antonellis KJ, Scherf U, et al. Exploration, normalization, and summaries of high density oligonucleotide array probe level data. Biostatistics (Oxford, England) 2003;4(April (2)):249–64.
[17] Wu Z, Irizarry RA, Gentleman R, Martinez-Murillo F, Spencer F. A model-based background adjustment for oligonucleotide expression arrays. Journal of the American Statistical Association 2004:909–17.
[18] Smyth GK. Linear models and empirical bayes methods for assessing differential expression in microarray experiments. Statistical Applications in Genetics and Molecular Biology 2004;3 [Article 3].
[19] Benjamini Y, Hochberg Y. Controlling the false discovery rate: a practical and powerful approach to multiple testing. Journal of the Royal Statistical Society Series B (Methodological) 1995;57(1):289–300.
[20] Gentleman RC, Carey VJ, Bates DM, Bolstad B, Dettling M, Dudoit S, et al. Bioconductor: open software development for computational biology and bioinformatics. Genome Biology 2004;5(10):R80.
[21] Ihaka R, Gentleman R. R: a language for data analysis and graphics. Journal of Computational and Graphical Statistics 1996;5(3):299–314.
[22] Datta S, Datta S. Evaluation of clustering algorithms for gene expression data. BMC Bioinformatics 2006:S17.
[23] Chen Y, Hallenbeck JM, Ruetzler C, Bol D, Thomas K, Berman NE, et al. Overexpression of monocyte chemoattractant protein 1 in the brain exacerbates ischemic brain injury and is associated with recruitment of inflammatory cells. Journal of Cerebral Blood Flow and Metabolism 2003;23(June (6)):748–55.
[24] Liu T, Matsuguchi T, Tsuboi N, Yajima T, Yoshikai Y. Differences in expression of toll-like receptors and their reactivities in dendritic cells in BALB/c and C57BL/6 mice. Infection and Immunity 2002;70(December (12)):6638–45.
[25] Elhofy A, Wang J, Tani M, Fife BT, Kennedy KJ, Bennett J, et al. Transgenic expression of CCL2 in the central nervous system prevents experimental autoimmune encephalomyelitis. Journal of Leukocyte Biology 2005;77(February (2)):229–37.
[26] Kasai M, Yoneda T, Habu S, Maruyama Y, Okumura K, Tokunaga T. In vivo effect of anti-asialo GM1 antibody on natural killer activity. Nature 1981;291(May (5813)):334–5.
[27] Alevizatos AC, McKinney RW, Feigin RD. Live, attenuated Venezuelan equine encephalomyelitis virus vaccine. I. Clinical effects in man. The American Journal of Tropical Medicine and Hygiene 1967;16(November (6)):762–8.
[28] Simmons JD, White LJ, Morrison TE, Montgomery SA, Whitmore AC, Johnston RE, et al. Venezuelan equine encephalitis virus disrupts STAT1 signaling by distinct mechanisms independent of host shutoff. Journal of Virology 2009;83(October (20)):10571–81.
[29] White LJ, Wang J.-G., Davis NL, Johnston RE. Role of alpha/beta interferon in Venezuelan equine encephalitis virus pathogenesis: effect of an attenuating mutation in the 5′ untranslated region. Journal of Virology 2001;75(April (8)):3706–18.
[30] Jahrling PB, Navarro E, Scherer WF. Interferon induction and sensitivity as correlates to virulence of Venezuelan encephalitis viruses for hamsters. Archives of Virology 1976;51:23.
[31] Swann JB, Hayakawa Y, Zerafa N, Sheehan KC, Scott B, Schreiber RD, et al. Type I IFN contributes to NK cell homeostasis, activation, and antitumor function. Journal of Immunology 2007;178(June (12)):7540–9.
[32] Paessler S, Yun NE, Judy BM, Dziuba N, Zacks MA, Grund AH, et al. Alpha-beta T cells provide protection against lethal encephalitis in the murine model of VEEV infection. Virology 2007;367(October (2)):307–23.
[33] Yun NE, Peng BH, Bertke AS, Borisevich V, Smith JK, Smith JN, et al. $CD4^+$ T cells provide protection against acute lethal encephalitis caused by Venezuelan equine encephalitis virus. Vaccine 2009;27(June (30)):4064–73.
[34] Kamath AB, Alt J, Debbabi H, Taylor C, Behar SM. The major histocompatibility complex haplotype affects T-cell recognition of mycobacterial antigens but not resistance to *Mycobacterium tuberculosis* in C3H mice. Infection and Immunity 2004;72(December (12)):6790–8.
[35] Biron CA. More things in heaven and earth: defining innate and adaptive immunity. Nature Immunology 2010;11(December (12)):1080–2.
[36] Biron CA. Expansion, maintenance, and memory in NK and T cells during viral infections: responding to pressures for defense and regulation. PLoS Pathogens 2010;6(March (3)):e1000816.
[37] Lee SH, Miyagi T, Biron CA. Keeping NK cells in highly regulated antiviral warfare. Trends in Immunology 2007;28(June (6)):252–9.
[38] Alsharifi M, Lobigs M, Simon MM, Kersten A, Muller K, Koskinen A, et al. NK cell-mediated immunopathology during an acute viral infection of the CNS. European Journal of Immunology 2006;36(April (4)):887–96.
[39] Paessler S, Fayzulin RZ, Anishchenko M, Greene IP, Weaver SC, Frolov I. Recombinant sindbis/Venezuelan equine encephalitis virus is highly attenuated and immunogenic. Journal of Virology 2003;77(September (17)):9278–86.